PERIODICO di MINERALOGIA Volume 91, No. 5, 2022
ISSN: 0369-8963

Tribological Behavior of AA7075 Nanohybrid Composites at High Temperature

M.L.AJIN[1], J.JEBEEN MOSES[1*], M.PRIYA DHARSHINI[2]

[1]Department of Mechanical Engineering, St. Xavier's Catholic College of Engineering, Chunkankadai, Nagercoil-629003, Kanniyakumari District, Tamilnadu, India-629003
[2]Research Department of Physics, Holy Cross College (Autonomous), Nagercoil, Kanniyakumari District, Tamilnadu, India-629004
*[*1] Corresponding author- J. JEBEEN MOSES*

Abstract

In this research work, an attempt was made to reinforce AA7075 aluminium alloy with nanosized Boron Carbide (B_4C) and Silicon Carbide (SiC) particles through stir casting technique. The manufactured composites were tested for wear utilizing pin on disc apparatus at high temperature by varying %reinforcement, applied load, sliding distance and applied velocity. The results revealed that the composites exhibit lower wear rate owing to the formation of Mechanically Mixed Layer (MML) due to third body abrasion as confirmed through EDAX. At low temperature, wear occurred through abrasion; whereas at high temperature, it was due to shearing, wear shift from mild to severe when the load exceeds 20N. When the temperature exceeds 225°C, no MML was formed as most of the materials were removed from composites owing to its reduction in hardness, hence the pin exhibit severe wear. The composites were produced with the objective of reducing the wear rate which was achieved using the WASPAS and VIKOR optimization technique. Cracks, pits and resolidified materials are some of the features observed on the worn surface morphology.

Keywords— *Stir Casting · High Temperature ·Wear · VIKOR · WASPAS · Worn surface morphology*

INTRODUCTION

Aluminum Metal Matrix Composite (AMMC) is gaining its importance in aerospace sector owing to its enhanced material properties and strength to weight ratio [1]. Composites are made using a variety of processes including power sintering, in-situ manufacturing and liquid metallurgy [2]. Manufacturing through liquid stir casting is the most cost-effective and suitable for large production of these processes [3]. The homogenous distribution of composites is influenced by numerous parameters such as particle size, volume percentage, particle shape and surface treatment [4]. The most often utilized reinforcing materials were Boron Carbide (B4C), Silicon Carbide (SiC), Aluminum oxide (Al_2O_3), Graphite (Gr), and Carbon Nanotubes (CNT) [5]. The major issue of AMMC is wettability of particles over the matrix material [6]. The wettability of composites is improved by adding flux. In comparison to untreated particles, heat-treated particles mix uniformly [29].

The existence of a mechanical mixed layer enhances the wear resistance of composites by preventing direct metal-to-metal contact [7]. The weight % and counter face stiffness have a negative impact on the wear rate, but the load and speed applied have a beneficial impact [8]. The duct surface has no influence on wear rate due to the presence of tribo substrate [9]. At lower loads, composite materials show abrasion and delamination wear, but at greater loads, they show severe wear [10]. The slowing of the subsurface increases with increased rush in the moderate wear area, but decreases when reinforcing particles are applied [11]. The presence of graphite activates the self-lubrication feature, which is required for components that frequently require lubrication [12].

Basavarajappa et al. [13] investigated the tribological characteristics of silicon carbide and graphite enhanced hybrid composites. Stir casting was used to make the AA2219 hybrid composites with different volume fractions. Variations in sliding speed and load were carried out to conduct the wear test. The results demonstrated that the composites outperform unreinforced composites in terms of wear resistance. Surappa et al. [14] investigated the effect of the strengthening percentage, sliding velocity, loading and sliding distance on wear using complete factor design. They presented a regression equation that showed wear reinforcing dependency, sliding velocity, load and sliding lengths and wear dependence.

The challenge of determining and picking the best answer based on contradicting characteristics in a large variety of possibilities is constantly present in the manufacturing industry. WASPAS (Weighted Aggregated Sum–Product Assessment) and VIKOR was a Multi Criteria Decision Making approach (MCDM) that is used to choose the best choice from a set of options. Each classification issue consists primarily of four main components: (a) equivalents, (b) abilities, (c) a significant weight for each attribute and (d) different output measures in connection to various characteristics [15, 16]. According to the results of the survey, a great deal of effort has gone into improving the material qualities by adding reinforcing particles. However, only a little amount of research has been done to improve the properties of the AA7075 aluminium alloy at high temperature reinforced with nanoparticles. The current study used a Stir casting approach to strengthen AA7075 aluminium alloy with Silicon Carbide (SiC) and Boron Carbide (B_4C) nanoparticles. The WASPAS and VIKOR techniques were used to improve the findings. The worn surface morphology was analyzed using the Scanning Electron Microscope (SEM).

Experimental Procedure

Material Preparation

The matrix material, AA7075 aluminium alloy with the chemical composition shown in Table 1, was obtained from Perfect Metal Alloys in Bangalore. As reinforcement, SiC and B_4C particles with an average particle size of 5nm were chosen from the Bhukanvala sectors. The moisture content in the selected reinforcing particles was removed by heating them to a temperature of 250°C. In an electric furnace, a graphite crucible

 https://doi.org/10.37896/pd91.5/91514

ISSN: 0369-8963

was filled with 1 kilogramme of AA7168 and heated to 860°C. Potassium Titanium Fluoride (K_2TiF_6) powder was used as a flux to make the reinforcing particles more wettable. The charge has been added to the warmed reinforcement and swirled at 1000rpm. The charge was cooled to 500°C and agitated for another 120 seconds after being stirred for 180 seconds. The charge was heated to 860°C once again, swirled for 120 seconds and then poured into the prepared high carbon steel die. Table 2 lists the input variables for casting. The same process was used to create composites with different weight percentages (0%, 2.5%, 5%, 7.5% & 10%). To eliminate surface imperfections, the composite surface was turned to a depth of 2mm.

Table 1 Chemical configuration of AA7075 Aluminium Alloy

Al	Zn	Mg	Cu	Fe	Zr	Si	Ti
87.81	5.6	2.8	3.2	0.22	0.15	0.12	0.1

Table 2 Stir Casting input variables

Casting temperature	860°C
SiC preheating temperature	250°C
B_4C preheating temperature	250°C
Die preheating temperature	400°C
Stirring Speed (RPM)	1000
Stirring time (Sec)	420
Flux	K_2TiF_6

Characterization

The pin on disc experiments were carried out on the composites according to ASTM G99 standards by adjusting the temperature (°C), load (N), sliding speed (m/s) and sliding distance (m) as indicated in Table 3. The composites' hardness was evaluated using ASTM E18 standards. The obtained results were optimized using the WASPAS and VIKOR optimization technique.

Table 3 Wear input variables and its levels

Process Parameters	Levels
Weight percentage of B_4C	5
Weight percentage of SiC	0, 2.5, 5, 7.5, 10
Load (N)	12, 24, 36, 48, 60
Speed (m/s)	1.5, 3.0, 4.5, 6.0, 7.5
Distance (m)	1000, 2000, 3000, 4000, 5000
Temperature (°C)	75, 150, 225, 300, 375

Results and Discussion

Microstructure

The microstructure of the composites was analyzed through SEM with EDAX mapping, in which each element was differentiated with the distinct colors. The Elemental analysis revealed that the incorporated SiC and B_4C nanoparticles were uniformly dispersed over the matrix materials as shown in the Fig.1. The Titanium element present in the flux coated over the nanoparticles had improved the wettability of reinforced particles over the matrix materials [17]. The hardness of the AA7075 hybrid composites increased with raise in the weight percentage of the reinforced particles as depicted in the Fig.2. The potassium present in the flux removes the impurities as slag; whereas fluoride escapes as white fumes and Titanium surrounds the reinforced nanoparticles and facilitates the wettability and also refines the grains of the AA7075 alloy [18]. It follows the Hall-Petch relation which states that when a material's grain size decreases, grain boundaries prevent dislocations from migrating, hence hardness increases.

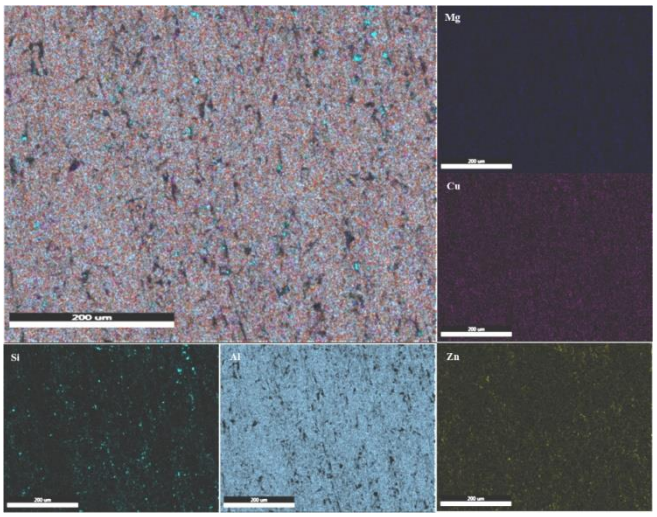

Fig. 1 Elemental Analysis of AA7075 hybrid nanocomposites

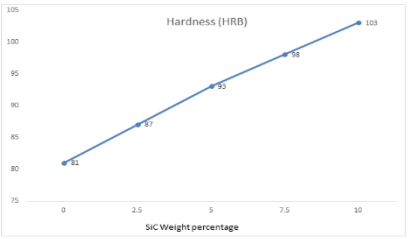

Fig. 2 Hardness of AA7075 with varying SiC content

Wear Rate

The wear rate of the composites reduces with increase in the weight percentage of the SiC particles as depicted in the Fig.3. The reinforced particles in the composites detach from the surface during sliding and enter the sliding regime, resulting in third body abrasion, which erodes the material from the composite pin as well as the counter face due to its abrasive nature. The eroded material generates the Mechanically Mixed Layer (MML), which prevents the direct metal to metal contact and ultimately reduces the wear rate [19]. The presence of oxygen in the EDAX study revealed that the oxide layer separated the contact surfaces, reducing metal-to-metal contact. Although oxidation will occur after the particles have been torn away from the wear surface, it is likely that atleast a percentage of the oxides identified in debris were generated while the particles were bonded to the substrate at the contact interface [20]. Fig.4 shows the presence of ferrous and the transfer of iron from the disc to the pin's surface, resulting in the development of MML.

When the reinforcing weight percentage exceeds 7.5%, agglomeration of particles occurred resulting in the reduction of wear resistance, similar trends were reported by the distinct researchers. The rate of wear increases as the temperature rises and the line rises linearly from the origin [21]. The wear processes in this area are typical of severe wear, involving the deposition of a composite transfer layer on the tool steel ring and substantial intermetallic welding. When sliding at the temperature of 225°C, the pin reached a maximum temperature of 470°C during sliding, as measured through thermos couple, which was higher than the

https://doi.org/10.37896/pd91.5/91514

ISSN: 0369-8963

deformation temperature of AA7075, hence more material was lost from the pin as a consequence of third body abrasion. Many researchers have found that when the applied load increases, the wear rate increases well corelated with the experimental findings.

The shift from mild to severe wear rate transpired at a load of 24 N, similar to the research findings of Bauri et al. [22] claimed that the transition ensues at a load of 20 N. But composites flaunt mediocre wear rate until 65 N; at high loads, the particles impose more compressive force, resulting in thicker MML and hence higher wear resistance [30]. The wear rate increases with upsurge in velocity until the saddle point of 3m/s thereafter it reduces, acclaimed to the fact reduction of Co-efficient Of Friction (COF). The heat generated during sliding aided in the creation of tribo-rich MML, positioned between the surface and avoids direct contact, lowering the wear rate [23]. The wear rate reduces with increase in the sliding distance which was contradictory to the results observed by the several researchers. Increased sliding distance causes the materials to soften and a tribo-oxide layer to develop. As a result, COF may increase owing to softening, but it will tend to decrease as the tribo-oxide coating forms and the wear rate decreases [24].

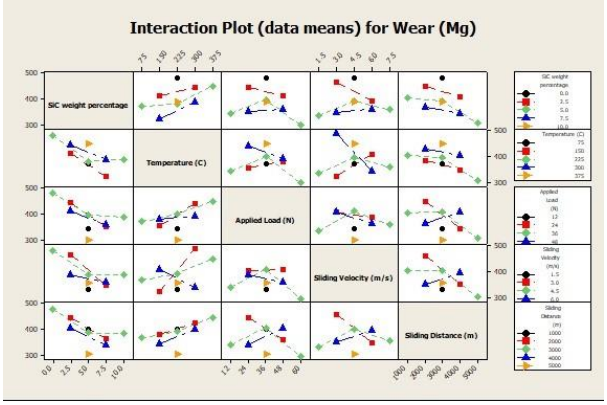

Fig. 3 Interaction of various process parameters on AA7075 hybrid nanocomposites

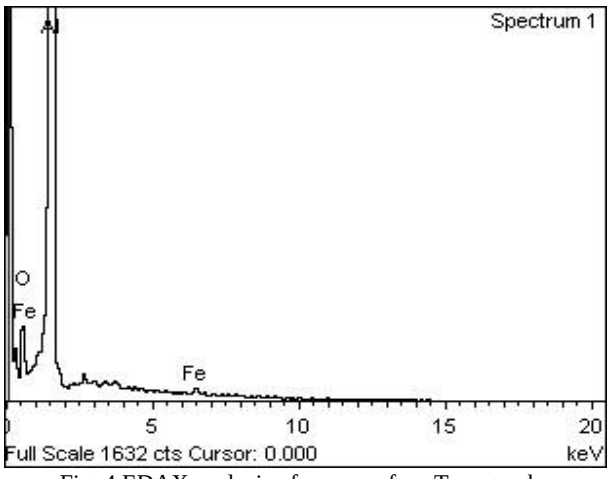

Fig. 4 EDAX analysis of worn surface Topography

Optimization Approaches

WASPAS

The WASPAS optimization approach was used to determine the ideal weight % of reinforcing particles. The initial stage was to create a decision matrix; in this case, 32 tests were carried out with four input variables, and wear and friction were recorded as responses, resulting in a 32x2 decisive matrix as given in Table 4.

$$N_{ij} = W_{ij}\left(\sum_{j=1}^{n}\frac{X_{ij}}{Max(X_{ij})}\right) \quad \ldots (1)$$

$$T_{1_{ij}} = \sum_{i=1}^{n} N_{ij} \quad \ldots (2)$$

In the next phases, the crucial matrix was normalized. From the provided replies, the maximum and minimum values were determined [25]. For beneficiary attributes, this normalization value was the ratio of the highest value of the decision matrix column to the individual variable contained in that column, and for non-beneficiary attributes, it was the ratio of the individual element to the lowest value. To produce a weighted normalized matrix, the normalized value was multiplied by the weight of each condition, as shown in equation 1.

$$M_{ij} = \left(\sum_{j=1}^{n}\frac{X_{ij}}{Max(X_{ij})}\right)^{W_{ij}} \quad \ldots (3)$$

$$T_{2_{ij}} = \prod_{i=1}^{n} M_{ij} \quad \ldots (4)$$

As shown in Table 5, the taxation component one was equal to the total of the weighted normalized matrix values [26]. The normalized value was squared with the weight of the matching answer, and the result was multiplied by each other to compute the taxation value two, as specified in equations 3 and 4. The assessment value was the sum of taxation value one to the lambda and taxation value two of the discrepancy between unit value and lambda, as indicated in equation 5. The best parameters were picked based on their highest assessment value.

$$A_{ij} = \sum_{i=1}^{n}\left(\lambda\left(T1_{ij}\right) + (1-\lambda)\left(T2_{ij}\right)\right) \quad \ldots (5)$$

VIKOR

The VIKOR optimization approach was used to identify the parametric combination. The formation choice matrix A_{ij} is the initial stage, where i denotes the number of replies and j denotes the number of experimental runs [27]. In the current study, a 32x2 decision matrix was created, as shown in Table 4. The equation 6 was used to normalize the decision matrix.

$$X_{ij} = \frac{(A_{ij})^2}{\sqrt{\sum_{j=1}^{n}(A_{ij})2}} \quad (6)$$

$$Y_i = \sum_{j=1}^{n} W_j\left[\left(X_{ij}\right)_{max} - \left(X_{ij}\right)\right] / \left[\left(X_{ij}\right)_{max} - \left(X_{ij}\right)_{min}\right] \quad (7)$$

The next step is to use the normalized matrix to calculate the best and worst values for all criterions, as shown in equations 7 and 8, where Y_i-max) is Y_i's maximum value and Y (i-min) is Y_i's minimum value; Z_i-max is Z_i's highest value, and Z_i-min is Zi's least value. v is the weight of the majority of criteria approach, which is normally set to 0.5 and has a value between 0 and 1. To generate ranking lists, the values of Y_i, Z_i, and P_i as well as the alternatives [28] are independently ordered and the values are gotten from 0 to 1 using equation 9 as shown in Table 6.

$$Z_i = Max^n of\left\{w_j\left[\left|\left(X_{ij}\right)_{max} - \left(X_{ij}\right)\right|\right] / \left[\left(X_{ij}\right)_{max} - \left(X_{ij}\right)_{min}\right]\right\} j = 1,2,\ldots,n \quad (8)$$

$$P_i = \frac{v((Y_i - Y_{i-min}))}{((Y_{i-max} - Y_{i-min}))} + (1-v)\left(\left(\frac{((Z_i - Z_{i-min}))}{((Z_{i-max} - Z_{i-min}))}\right)\right) \quad (9)$$

The optimization technique revealed that alloy reinforced with 2.5% of nanoparticles were suitable for sliding

https://doi.org/10.37896/pd91.5/91514

ISSN: 0369-8963

application at 300°C whereas 7.5% of reinforcing content was suitable for applications at 150°C.

Table 4 Decision matrix and worn experimental results of AA7075 nanohybrid composites

S.No.	SiC (Wt %)	Temp °C	Applied Load (N)	Sliding Velocity (m/s)	Sliding Distance (m)	Wear (mg)	COF
1	5	225	60	4.5	3000	295.139	0.428311
2	5	225	36	4.5	3000	464.11	0.340236
3	2.5	150	24	6	2000	458.401	0.391387
4	5	75	36	4.5	3000	367.473	0.338763
5	7.5	300	24	6	2000	361.715	0.363987
6	5	225	36	4.5	3000	331.987	0.364473
7	2.5	300	24	6	4000	371.166	0.385131
8	2.5	150	24	3	4000	283.687	0.378442
9	5	225	36	4.5	5000	302.935	0.370153
10	7.5	150	48	3	4000	269.156	0.371887
11	5	225	36	1.5	3000	332.43	0.368062
12	2.5	150	48	6	4000	480.326	0.363289
13	7.5	150	48	6	2000	337.817	0.404193
14	7.5	300	48	3	2000	441.484	0.347619
15	5	375	36	4.5	3000	447.857	0.378826
16	10	225	36	4.5	3000	386.176	0.399911
17	5	225	36	4.5	3000	487.366	0.359405
18	2.5	300	24	3	2000	658.638	0.355776
19	7.5	300	24	3	4000	360.056	0.354872
20	7.5	150	24	3	2000	314.05	0.335815
21	2.5	300	48	3	4000	493.211	0.390621
22	5	225	36	4.5	3000	498.946	0.395977
23	2.5	150	48	3	2000	421.537	0.367221
24	5	225	36	7.5	3000	355.562	0.360014
25	0	225	36	4.5	3000	479.16	0.373042
26	5	225	36	4.5	3000	444.289	0.373314
27	7.5	300	48	6	4000	379.689	0.335239
28	5	225	36	4.5	3000	286.09	0.367648
29	2.5	300	48	6	2000	242.012	0.35007
30	5	225	12	4.5	3000	341.246	0.376584
31	5	225	36	4.5	1000	402.803	0.382395
32	7.5	150	24	6	4000	352.234	0.360674
						W_{ij}	0.7	0.3

Table 5 Optimized value obtained through WASPAS optimization technique

Normalized decision matrix		Weighted normalised decision matrix		Appraisal Value 1	Normalized decision matrix		Appraisal Value 2	Assessment Value	Rank
0.819 99329	0.782 69995	0.573 9953	0.234 80999	0.8088 0529	0.870 29644	0.929 13451	0.8086 22464	0.808 71	7
0.521 45397	0.985 31314	0.365 01778	0.295 59394	0.6606 11717	0.633 94442	0.995 5711	0.6311 36743	0.645 87	23
0.527 94824	0.856 54097	0.369 56377	0.256 96229	0.6265 26057	0.639 46082	0.954 60662	0.6104 33533	0.618 48	26
0.658 58444	0.989 59745	0.461 00911	0.296 87923	0.7578 88342	0.746 49693	0.996 8678	0.7441 58756	0.751 02	13
0.669 06819	0.921 01916	0.468 34773	0.276 30575	0.7446 5348	0.754 79544	0.975 61979	0.7363 93364	0.740 52	16
0.728 98035	0.919 79104	0.510 28625	0.275 93731	0.7862 23558	0.801 49548	0.975 22933	0.7816 41894	0.783 93	8
0.652 03171	0.870 45447	0.456 42219	0.261 13634	0.7175 58534	0.741 28993	0.959 23235	0.7110 69282	0.714 31	18
0.853 09514	0.885 83984	0.597 1666	0.265 75195	0.8629 18547	0.894 74283	0.964 28756	0.8627 89375	0.862 85	4
0.798 89085	0.905 67684	0.559 2236	0.271 70305	0.8309 26648	0.854 55735	0.970 71553	0.8295 32092	0.830 23	6
0.899 15142	0.901 45394	0.629 406	0.270 43618	0.8998 42176	0.928 28853	0.969 35546	0.8998 41558	0.899 84	2
0.728 0089	0.910 82209	0.509 60623	0.273 24663	0.7828 5286	0.800 74767	0.972 36668	0.7786 2035	0.780 74	9
0.503 84947	0.922 78874	0.352 69463	0.276 83662	0.6295 31251	0.618 88586	0.976 18176	0.6041 4509	0.616 84	27
0.716 39971	0.829 40328	0.501 4798	0.248 82098	0.7503 00779	0.791 78775	0.945 43075	0.7485 80491	0.749 44	14
0.548 17842	0.964 3863	0.383 72489	0.289 31589	0.6730 4078	0.656 51606	0.989 17996	0.6494 12527	0.661 23	22
0.540 37784	0.884 9419	0.378 26449	0.265 48257	0.6437 47061	0.649 96246	0.963 99421	0.6265 60051	0.635 15	25
0.626 68835	0.838 28402	0.438 68184	0.251 48521	0.6901 6705	0.721 00144	0.948 45637	0.6838 3841	0.687	19
0.496 57137	0.932 76109	0.347 59996	0.279 82833	0.6274 28283	0.612 61436	0.979 33466	0.5999 54475	0.613 69	28
0.367 44312	0.942 27548	0.257 21018	0.282 68264	0.5398 92825	0.496 17295	0.982 32086	0.4874 01037	0.513 65	32
0.672 151	0.944 67583	0.470 5057	0.283 40275	0.7539 08447	0.757 22823	0.983 0709	0.7444 09033	0.749 16	15
0.770 61614	0.998 28477	0.539 4313	0.299 48543	0.8389 16732	0.833 27178	0.999 48512	0.8328 42743	0.835 88	5
0.490 68654	0.858 22063	0.343 48058	0.257 46619	0.6009 46768	0.607 52325	0.955 16782	0.5802 86661	0.590 62	30
0.485 04648	0.846 6123	0.339 53253	0.253 98369	0.5935 16226	0.602 62667	0.951 27344	0.5732 62748	0.583 39	31
0.574 11805	0.912 90803	0.401 88263	0.273 87241	0.6757 55044	0.678 11108	0.973 03421	0.6598 25277	0.667 79	21
0.680 64641	0.931 18323	0.476 45249	0.279 35497	0.7558 07459	0.763 9151	0.978 83738	0.7477 48648	0.751 78	12
0.505 07555	0.898 66289	0.353 55288	0.269 59887	0.6231 5175	0.619 93969	0.968 4541	0.6003 83133	0.611 77	29
0.544 71751	0.898 00811	0.381 30226	0.269 40243	0.6507 04694	0.653 61188	0.968 24236	0.6328 54709	0.641 78	24
0.637 39534	1	0.446 17674	0.3	0.7461 76739	0.729 60234	1	0.7296 02343	0.737 89	17
0.845 9296	0.911 84775	0.592 15072	0.273 55432	0.8657 05046	0.889 47543	0.972 69503	0.8651 88334	0.865 45	3
1	0.957 63419	0.7	0.287 29026	0.9872 90256	1	0.987 09714	0.9870 97138	0.987 19	1
0.709 20099	0.890 21042	0.496 44069	0.267 06313	0.7635 03816	0.786 20994	0.965 71239	0.7592 5268	0.761 38	10
0.600 81976	0.876 68249	0.420 57383	0.263 00475	0.6835 78575	0.700 03692	0.961 28618	0.6729 35814	0.678 26	20
0.687 07734	0.929 47925	0.480 95414	0.278 84378	0.7597 97914	0.768 96033	0.978 29968	0.7522 73647	0.756 04	11

Table 6 Optimized value obtained through VIKOR optimization technique

Normalized Decision matrix		Weighted normalized decision matrix		Assessment value	Rank
0.130929	0.204434	0.03725839	0.20443367	0.67412678	29
0.205887	0.162395	0.15575912	0.01097597	0.45738543	20
0.203355	0.18681	0.15175535	0.1233297	0.62746238	28
0.163017	0.161692	0.08798681	0.0077405	0.21034214	5
0.160463	0.173732	0.08394868	0.0631453	0.28685073	14
0.147275	0.173964	0.06310019	0.0642128	0.21638161	6
0.164656	0.183824	0.09057674	0.10958833	0.42331518	16
0.125848	0.180631	0.02922701	0.09489586	0.27024232	13
0.134387	0.176675	0.04272579	0.07668898	0.22745067	7
0.119402	0.177502	0.01903631	0.08049773	0.20216459	4
0.147472	0.175677	0.06341087	0.07209608	0.24500994	9
0.213081	0.173399	0.16713153	0.06161213	0.58103658	25
0.149861	0.192922	0.06718882	0.15145822	0.53428269	22
0.19585	0.165919	0.13989132	0.02719281	0.42739694	17
0.198677	0.180814	0.14436076	0.09573932	0.5558147	23
0.171314	0.190878	0.10110338	0.14205276	0.5563841	24
0.216204	0.171545	0.17206874	0.05308088	0.58464824	26
0.292183	0.169813	0.29218317	0.04510975	1	32
0.159727	0.169381	0.08278521	0.0431241	0.24984862	10
0.139318	0.160285	0.05052083	0.00126519	0.06608109	2
0.218797	0.186444	0.17616788	0.12164717	0.71177766	30
0.221341	0.189001	0.18018989	0.13341168	0.74542761	31
0.187001	0.175275	0.12590233	0.07024881	0.44814947	18
0.157733	0.171835	0.07963353	0.05441856	0.25713976	12
0.212564	0.178054	0.1663138	0.08303471	0.61327151	27
0.197094	0.178183	0.14185849	0.08363216	0.52702318	21
0.168437	0.16001	0.09655399	0	0.2281989	8
0.126914	0.175479	0.03091226	0.07118672	0.18844041	3
0.107361	0.167089	0	0.03257645	0	1
0.151383	0.179744	0.0695936	0.09081475	0.32192186	15
0.17869	0.182518	0.11276402	0.10357867	0.45597693	19
0.156257	0.17215	0.07729958	0.05586826	0.25119364	11

Worn surface morphology

The worn surface morphology of AA7075 nano composites tested at the temperature of 75°C was shown in the Fig.5a. The scratches are visible throughout the surface which conforms that abrasion was the dominant mode of wear which occurred due to the detachment of reinforced particles. With the applied load these particles penetrate deep inside the alloy and tear it hence the wear rate increases. At higher magnification of

https://doi.org/10.37896/pd91.5/91514

ISSN: 0369-8963

2000X, it was evident that the materials were glued on the edges of the scratches which confirmed that adhesive wear occurred as depicted in the figure 5b. Wear debris in the form of particles was sticked back to the surface inside the ripped zone, confirming that the material was brittle in nature. When slides at the temperature of 150°C, the material starts to flow but lot of abrasion marks are clearly visible confirming that the mode of wear was adhesion and abrasion, of which later was dominant. The materials were plastically deformed which was evident that the ductility of materials increased as depicted in the figure 6a. At higher magnification, the reinforced particles penetrated deep inside the material and a hug crack occurred. A white line was observed, which confirmed that the materials were remelted over the surface as depicted in the Fig. 6b.

At the temperature of 225°C, the delamination wear was evident and the crack occurred perpendicular to the direction of slide confirming that the mode of wear was adhesive as shown in the Fig.7a. The average width of the crack was 1µm and inside the wear regime numerous numbers of micro pits were clearly visible. At higher magnification, A Type-I crack was observed, which has a common origin point but has different end point as portrayed in the Fig. 7b. The materials were dugged out from the surface and the average width of the crack was around 3µm near the delamination region. At the temperature of 300°C materials were welded on the surface and the average size of the worn debris ranges from 25µm to 30µm as shown in the Fig. 8a. The scratches were observed on the surface, whereas pits and cracks were not visible confirmed that the mode of wear was shearing. At higher magnification Fig. 8b, materials flow and adhesion on the surface was evident, and a larger volume of wear debris were attached to the surface confirmed that the materials attained its deformation temperature during sliding. At 375°C, materials flow plastically, owing to its soft nature, it exhibits lower COF, third body abrasion removes maximum materials from the softer aluminium hence MML was not formed results in severe wear rate as portrayed in the Fig.9a. At higher magnification, the materials were sheared and plastically deformed and welded on the surface as shown in the Fig.9b.

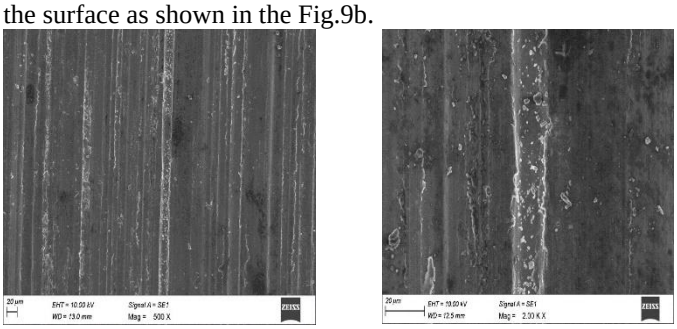

Fig. 5 Worn surface topography of AA7075 nanocomposites tested at 75°C (a) at 500X (b) at 2000X

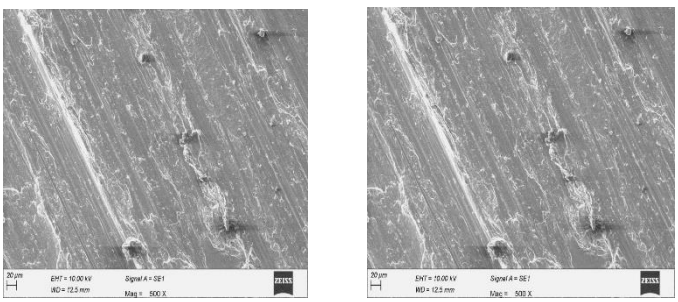

Fig. 6 Worn surface topography of AA7075 nanocomposites tested at 150°C (a) at 500X (b) at 2000X

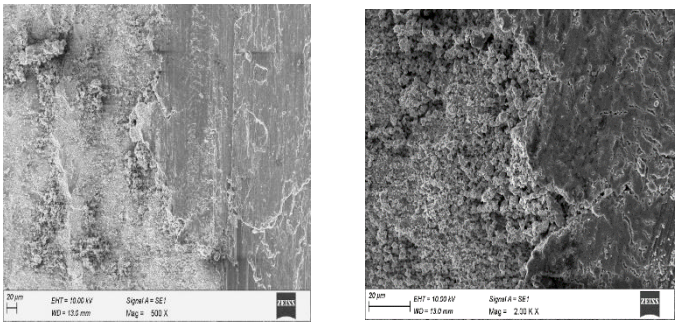

Fig. 7 Worn surface topography of AA7075 nanocomposites tested at 225°C (a) at 500X (b) at 2000X

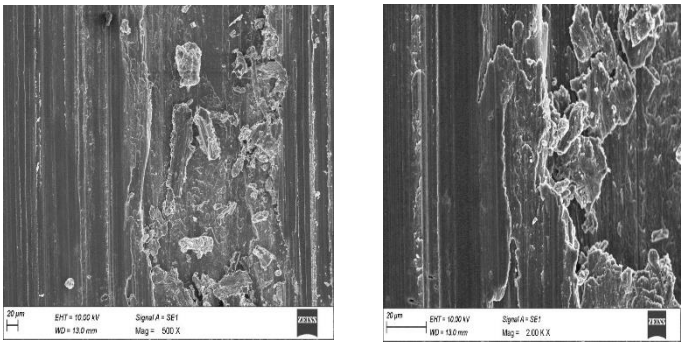

Fig. 8 Worn surface topography of AA7075 nanocomposites tested at 300°C (a) at 500X (b) at 2000X

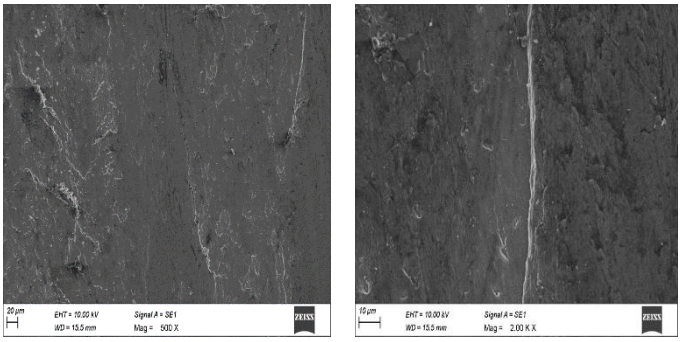

Fig. 9 Worn surface topography of AA7075 nanocomposites tested at 375°C (a) at 500X (b) at 2000X

Conclusions

The AA7075/SiC/B_4C nanohybrid composites were successfully fabricated through stir casting technique and following conclusion were obtained.

1. The particles were uniformly dispersed over the matrix material and it was confirmed through SEM with EDS mapping. The hardness of the composites increases with raise in weight percentage of composites owing to the Hall Petch effect.
2. With the addition of reinforcing particles, enhancement in wear resistance was observed owing to the formation of MML, no MML was formed at higher temperature leads to the severe wear rate. At low temperature, the mode of wear was Abrasive, it was adhesive at high temperature, transition from mild to severe wear occurred at the load of 20N.
3. At low temperature, scratches, brittle tear, cracks were observed on the worn surface morphology, whereas at high temperature plastic deformation, adhesion and material welding on the surface was evident.
4. The optimization results confirmed that alloy reinforced with 2.5% of nanoparticles were suitable for sliding

https://doi.org/10.37896/pd91.5/91514

ISSN: 0369-8963

application at 300°C whereas 7.5% of reinforcing content was suitable for applications at 150°C.

References

[1] Idusuyi, N., & Olayinka, J.I. (2019). "Dry sliding wear characteristics of aluminium metal matrix composite". Journal of Materials Research and Technology, 8(3), 3338-3346.

[2] Srivastava, A. K., Dixit, A. R., & Tiwari, S. (2018). "A review on the intensification of metal matrix composites and its nonconventional machining". Science and Engineering of composite materials, 25(2), 213-228.

[3] Samal, P., Vundavilli, P. R., Meher, A., & Mahapatra, M. M. (2020). "Recent progress in aluminum metal matrix composites: A review on processing, mechanical and wear properties". Journal of Manufacturing Processes, 59, 131-152.

[4] Pazhouhanfar, Y., & Eghbali, B. (2018). "Microstructural characterization and mechanical properties of TiB2 reinforced Al6061 matrix composites produced using stir casting process". Materials Science and Engineering A, 710, 172-180

[5] Bhoi, N. K., Singh, H., & Pratap, S. (2020). "Developments in the aluminum metal matrix composites reinforced by micro/nano particles–a review". Journal of Composite Materials, 54(6), 813-833.

[6] Malaki, M., Fadaei Tehrani, A., Niroumand, B., & Gupta, M. (2021). "Wettability in metal matrix composites". Metals, 11(7), 1034.

[7] Nageswaran, G., Natarajan, S., & Ramkumar, K.R. (2018). "Synthesis, structural characterization, mechanical and wear behaviour of Cu-TiO2-Gr hybrid composite through stir casting technique". Journal of Alloys and Compounds, 768, 733-74.

[8] Hillary, J.J.M., Ramamoorthi, R., & Chelladurai, S.J.S. (2020). "Dry sliding wear behaviour of Al6061–5% SiC—TiB2 hybrid metal matrix composites synthesized by stir casting process". Materials Research Express, **7**(12), 126519.

[9] Alam, M.T., Arif, S., Ansari, A.H., & Alam, M.N. (2019). "Optimization of wear behaviour using Taguchi and ANN of fabricated aluminium matrix nanocomposites by two-step stir casting". Materials Research Express, 6(6), 065002.

[10] Ranjith, R., Giridharan, P.K. Devaraj, J. & Bharath, V. (2017). "Influence of titanium-coated (B4Cp+ SiCp) particles on sulphide stress corrosion and wear behaviour of AA7050 hybrid composites (for MLG link)". Journal of the Australian Ceramic Society, 53(2), 1017-1025.

[11] Singh, H., Haq, M.I.U., & Raina, A. (2020). "Dry sliding friction and wear behaviour of AA6082-TiB2 in situ composites". Silicon, 12(6), 1469-1479.

[12] Ranjith, R., Giridharan, P.K., Velmurugan, C., & Chinnusamy, C. (2019). "Formation of lubricated tribo layer, grain boundary precipitates, and white spots on titanium-coated graphite–reinforced hybrid composites". Journal of the Australian Ceramic Society, 55(3), 645-655.

[13] Basavarajappa, S., Chandramohan, G., Mukund, K., Ashwin, M., & Prabu, M. (2006). "Dry sliding wear behavior of Al 2219/SiCp-Gr hybrid metal matrix composites". Journal of Materials Engineering and Performance, 15(6), 668-674.

[14] Surappa, M.K., (2008). "Synthesis of fly ash particle reinforced A356 Al composites and their characterization, Materials Science and Engineering A, 480(1-2), 117-124.

[15] Kutlu Gundogdu, F., Kahraman, C. (2019). "Extension of WASPAS with spherical fuzzy sets". Informatica, 30(2), 269-292.

[16] Lin, M., Chen, Z., Xu, Z., Gou, X., & Herrera, F. (2021). "Score function based on concentration degree for probabilistic linguistic term sets: an application to TOPSIS and VIKOR". Information Sciences, 551, 270-290.

[17] Ranjith, R., & Vimalkumar, S.N. (2021). "Integrated MOORA-ELECTRE approach for solving multi-criteria decision problem" World Journal of Engineering, 8, 1168-1172.

[18] Bharath, V., Auradi, V., Nagaral, M., & Boppana, S.B. (2020). "Experimental investigations on mechanical and wear behaviour of 2014Al–Al2O3 Composites". Journal of Bio-and Tribo-Corrosion, 6(2), 1-10.

[19] Ranjith, R., & Giridharan, P.K. (2017). "Influence of high temperature on surface hardness of AA7050 hybrid composites". Journal of Materials and Environmental Science 8, 1168-1172.

[20] Bhowmik, A., Dey, D., & Biswas, A. (2021). "Microstructure, mechanical and wear behaviour of Al7075/SiC aluminium matrix composite fabricated by stir casting" Indian Journal of Engineering and Materials Sciences (IJEMS), 28(1), 46-54.

[21] Kumar, A., Kumar, S., Mukhopadhyay, N.K., Yadav, A., Kumar, V., & Winczek, J. (2021). "Effect of variation of SiC reinforcement on wear behaviour of AZ91 alloy composites". Materials, 14(4), 990.

[22] Dipankar, D., Bhowmik, A., & Biswas, A. (2021). "Influence of TiB2 addition on friction and wear behaviour of Al2024-TiB2 ex-situ composites" Transactions of Nonferrous Metals Society of China, 31(5), 1249-1261.

[23] Ranjith, R., & Giridharan, P.K. (2015). "Experimental investigation of surface hardness and dry sliding wear behavior of AA7050/B 4 C p, High Temperature Material Processes". An International Quarterly of High-Technology Plasma Processes, 19(3-4).

[24] Sharath, B.N., & Venkatesh, C.V. (2021). "Study on Effect of boron carbide, aluminium oxide and graphite on dry sliding wear behaviour of aluminium based metal matrix composite at different temperature". Tribologia-Finnish Journal of Tribology, 38(1-2), 35-46.

[25] Ali, J., Bashir, Z., & Rashid, T. (2021). "WASPAS-based decision making methodology with unknown weight information under uncertain evaluations". Expert Systems with Applications, 168, 114143.

[26] Mishra, A.R., & Rani, P. (2021). "Multi-criteria healthcare waste disposal location selection based on Fermatean fuzzy WASPAS method". Complex & Intelligent Systems, **7**(5), 2469-2484.

[27] Bakioglu, G., & Atahan, A.O. (2021). "AHP integrated TOPSIS and VIKOR methods with Pythagorean fuzzy sets to prioritize risks in self-driving vehicles". Applied Soft Computing, 99, 106948.

[28] Lin, M., Chen, Z., Xu, Z., Gou, X., & Herrera, X, F. (2021). "Score function based on concentration degree for

 https://doi.org/10.37896/pd91.5/91514

ISSN: 0369-8963
probabilistic linguistic term sets an application to TOPSIS and VIKOR". Information Sciences 551, 270-290.

[29] Gutema, E.M., Bazhin, V.Y., & Fedorov, S.N. (2019). "Wettability enhancement of aluminum metal matrix composite reinforced with magnesium coated silicon carbide particles". Materials Science and Engineering, 560, 012179.

[30] Loganathan, P., Gnanavelbabu, A., & Rajkumar, K. (2021). "Influence of ZrB2/hBN particles on the wear behaviour of AA7075 composites fabricated through stir followed by squeeze cast technique". Journal of Engineering Tribology, 235(1), 149-160.

 https://doi.org/10.37896/pd91.5/91514